THE JOURNAL OF PHYSICAL CHEMISTRY Letters

Letter

Cite This: J. Phys. Chem. Lett. 2019, 10, 768−773

pubs.acs.org/JPCL

Monitoring Spontaneous Charge-Density Fluctuations by Single-Molecule Diffraction of Quantum Light

Konstantin E. Dorfman,*[,†] Shahaf Asban,*[,‡] Lyuzhou Ye,[‡] Jérémy R. Rouxel,[§,∥] Daeheum Cho,[‡] and Shaul Mukamel*[,‡]

[†]State Key Laboratory of Precision Spectroscopy, East China Normal University, Shanghai 200062, China

[‡]Department of Chemistry and Department of Physics and Astronomy, University of California, Irvine, California 92697-2025, United States

[§]Laboratory of Ultrafast Spectroscopy, École Polytechnique Fédérale de Lausanne, CH-1015 Lausanne, Switzerland

[∥]SwissFEL, Paul Scherrer Institut, 5232 Villigen, PSI, Switzerland

Supporting Information

ABSTRACT: Homodyne X-ray diffraction signals produced by classical light and classical detectors are given by the modulus square of the charge density in momentum space $|\sigma(\mathbf{q})|^2$, missing its phase, which is required in order to invert the signal to real space. We show that quantum detection of the radiation field yields a linear diffraction pattern that reveals $\sigma(\mathbf{q})$ itself, including the phase. We further show that repeated diffraction measurements with variable delays constitute a novel multidimensional measure of spontaneous charge-density fluctuations. Classical diffraction, in contrast, only reveals a subclass of even-order correlation functions. Simulations of two-dimensional signals obtained by two diffraction events are presented for the amino acid cysteine.

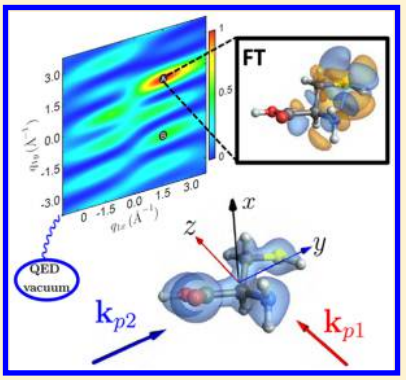

Photon counting, as described by the quantum theory of detection, is associated with the annihilation of a radiation mode.[1] Any detectable change in the number of photons requires at least two light−matter interactions. Diffraction of a classical source on quantum matter is thus a second-order process in the light−matter interaction. Setups with a low photon flux[2−8] or short wavelength[9−13] (that can detect the change in photon number) now exist.Taking the quantum nature of light into account is now called for.

Multidimensional diffraction can be measured by photon coincidence counting obtained by subjecting the molecule to sequences of pulses. The underlying matter information is given by the multipoint correlation functions of the charge density that governs the spontaneous charge fluctuations. The response and spontaneous fluctuations of both the field and charge density are mixed due to their quantum nature and classical response theory, which is causal and does not apply.[14] Thus, multidimensional spectroscopy, which involves several perturbations followed by a single measurement is fundamentally different from multidimensional diffraction, which consists of a series of measurements, and thus may not be retrieved simply by data processing of classical signals. Multidimensional diffraction carries new types of information related to spontaneous charge fluctuations, which is not accessible by classical light.[15]

In this Letter we consider off-resonant diffraction of nonclassical X-ray sources and explore phase-dependent quantum corrections to diffraction, involving a *single* light−matter interaction. Photons are not generated in this order (this requires two interactions), which only causes a phase change of the field. This results in a detectable photon intensity diffraction pattern when coupled to local quantum fluctuations at the detector. We denote this process as linear quantum diffraction (LQD) (i.e., linear in the charge density).

We consider an incoming light prepared either in a coherent state or in a Fock state interacting with a local field mode, which is eventually detected by photon annihilation in the detected mode.[1] Field intensity measurements show that local quantum fluctuations at the detector coupled to the detected mode generate signal linear in the charge density. Coherent (classical-like) or single-photon states provide higher degrees of spatial and spectral resolution, whereas an N-photon Fock state yields lower resolution.

Crystallographic signals generated by classical light are quadratic in the charge density in momentum space $\sigma(\mathbf{q})$. The phase is not available and phase reconstruction algorithms[16,17] or heterodyne detection[18] is required to retrieve the real-space charge density $\sigma(\mathbf{r}) = \int d\mathbf{q}\, e^{i\mathbf{q}\cdot\mathbf{r}}\sigma(\mathbf{q})$. Heterodyne detection of the signal field is achieved by interference with a local oscillator (LO),[19] which must be varied for each scattering angle. Phase

Received: January 9, 2019
Accepted: January 24, 2019
Published: January 24, 2019

DOI: 10.1021/acs.jpclett.9b00071
J. Phys. Chem. Lett. 2019, 10, 768−773

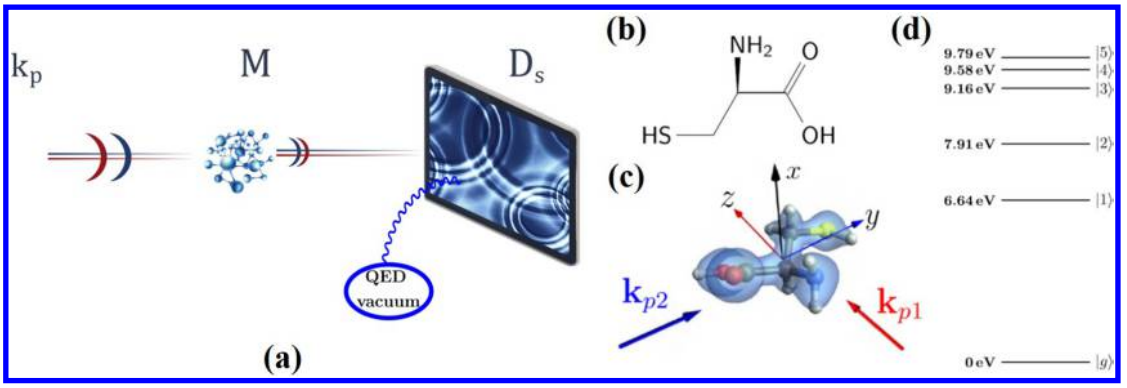

Figure 1. (a) The LQD setup. Single photon with momentum $\mathbf{k}_p$ diffracted off a single molecule and the LQD is detected on a screen (preparation pulse is not depicted). The blue circle represents the quantum vacuum fluctuations of QED that interacts once with the detector in the LQD scheme. (b) Chemical structure of cysteine. (c) Orientated cysteine and the ground state charge density σ_{gg}. The pulse configuration: $\mathbf{k}_{p1} \| \hat{z}$ and $\mathbf{k}_{p2} \| \hat{y}$. (d) Energy levels of the ground (g) and valence excited (e = 1, 2, ..., 5) states.

reconstruction algorithms usually require a reasonable initial guess in order to converge to the correct structure.[20,21] Signals linear in the charge density can reveal the phase of the Fourier-transformed charge densities and the crystallographic image. Thus, quantum detected diffraction offers an interesting possibility for overcoming the phase problem without scanning the LO for each detection angle. Furthermore, classical diffraction can be viewed as an ensemble average of different trajectories. Each detection event results from a trajectory terminated in a point at the detector. It is further blurred by the detector response function, even for an infinitesimal detection area (pixel size). Using quantum detection, this response can be studied at the single trajectory level, enhancing the resolution by reducing the spread and minimizing the noise.[22]

Repeated measurements involving sequences of n delayed pulses result in multiple diffraction signals each linear in the charge density given by n-dimensional correlation functions of the charge density. A classical diffraction experiment, in contrast, only reveals even order correlation functions.[23] Since the phase of the charge density in momentum space corresponds to translation in real space, correlation functions such as $\langle \sigma(\mathbf{q}_1,t_1)\, \sigma(\mathbf{q}_2,t_2)\rangle$ carry interesting structural−dynamical information that is inaccessible with classical light.

LQD Signal. Off-resonant diffraction is described by the minimal coupling matter/field interaction Hamiltonian,[24,25] $\mathcal{H}_I = \int d\mathbf{r}\ \sigma(\mathbf{r},t)\, \mathbf{A}^2(\mathbf{r},t)$, where σ is the charge-density operator while $\mathbf{A}$ is the vector potential. We first assume that the incoming light pulse is described by a multimode coherent state $|\psi_p(0)\rangle = \prod_{\mathbf{p},\lambda} |\alpha_{\mathbf{p},\lambda}\rangle$. Here $\alpha_{\mathbf{p},\lambda}$ represents the amplitude of the coherent state of a mode with momentum $\mathbf{p}$ and polarization λ. The diffraction pattern is obtained from the time-integrated spatially gated intensity at point $\mathbf{r}$ of the detector. Assuming no temporal gate $\tilde{F}_t^1(\bar{t},\omega) = 2\pi\delta(\omega)$ and performing rotational averaging $\langle \hat{\mathbf{r}}_m \hat{\mathbf{r}}_n \rangle = \delta_{m,n}/3$, the first-order expansion of the signal in eq S1 assumes the form

$$S_m^{(1)}[\mathbf{q}_{\{\mathbf{k}\}}(\mathbf{r})] \propto \mathcal{R}e \sum_{\mathbf{k},\mathbf{k}_p} \omega_{\mathbf{k}} \mathcal{E}_m^*(\mathbf{k})\, \mathcal{A}_m(\mathbf{k}_p) \tag{1}$$

$$\times \langle \sigma[\mathbf{q}_{\{\mathbf{k}\}}(\mathbf{r}),\omega_{\mathbf{q}}]\rangle e^{-i\mathbf{q}_{\{\mathbf{k}\}}(\mathbf{r})\cdot\mathbf{r}} \tag{2}$$

(1)

where m is a Cartesian component of the field, $\mathbf{q}_{\{\mathbf{k}\}}(\mathbf{r}) = \mathbf{k}_p - k\hat{\mathbf{r}}$ and $\omega_{\mathbf{q}} = \omega_{\mathbf{k}p} - \omega_{\mathbf{k}}$ are the diffraction wavector at a corresponding frequency, $\hat{\mathbf{r}}$ is a unit vector in the detection direction; the field and the vector potential amplitudes $\mathcal{E}_m(\mathbf{k})$ and $\mathcal{A}_n(\mathbf{k}_p)$ are given by expectation values of the corresponding operators (see eqs S6 and S7). The signal (eq 1), which depends on the momentum $\mathbf{k}$, is governed by the initial state configuration, polarization, and other degrees of freedom. The spatial resolution is controlled by the diffraction wavector $\mathbf{q}_{\{\mathbf{k}\}}(\mathbf{r})$; $\omega_{\mathbf{q}}$ can be a useful tool for monitoring transient states of the charge density. A similar result is obtained for a single-photon Fock state $|\psi_{1F}(0)\rangle = \sum_{\mathbf{p},\lambda} \Phi_{\mathbf{p},\lambda} |1_{\mathbf{p},\lambda}\rangle$ (see section S1 of the Supporting Information), where $\Phi_{\mathbf{p},\lambda}$ represents the Fock state amplitude.

Time-Resolved LQD. In this setup, an actinic pulse initially prepares the molecule in a superposition of electronic states and the LQD performed after a delay T probes the excited state dynamics. The superposition of electronic states is described by density matrix elements $\rho_{ab}^{(0)}$ with the phase $e^{i\phi_{ab}}$, where a and b are molecular electronic eigenstates. The impulsive diffraction off this state after time delay T is governed by the transition charge density element $\sigma_{ab} = \langle a|\hat{\sigma}|b\rangle$. The sum-over-states expression of eq 1 for a coherent or single photon state then reads

$$S_m^{(1)}[\mathbf{q}(\mathbf{r}),T] \propto \mathcal{R}e \sum_{\mathbf{k},\mathbf{k}_p} \sum_{a,b} \omega_{\mathbf{k}} \mathcal{E}_m^*(\mathbf{k})\, \mathcal{A}_m(\mathbf{k}_p)$$
$$\times \mathrm{Tr}\{\sigma_{ab}[\mathbf{q}(\mathbf{r}),\omega_{\mathbf{q}}]\rho_{ab}^{(0)}\} e^{-i\mathbf{q}(\mathbf{r})\cdot\mathbf{r}+i\phi_{ab}} \tag{3}$$

Thus, the LQD signal may reveal the single molecule coherence and its phase as well as the transient charge density and its phase.

We now turn to a different state of the incoming field: an N-photon Fock state described by the wave function $|\psi_{NF}(0)\rangle = \sum_{\mathbf{p},\lambda} \Phi_{\mathbf{p},\lambda}^{(N)} |N_{\mathbf{p},\lambda}\rangle$, where $\Phi_{\mathbf{p},\lambda}^{(N)}$ is the N-photon amplitude of the $\mathbf{p}$ mode with polarization λ. Assuming no temporal gating we obtain from eq S1 upon rotational averaging,

$$S_m^{(1)}[\mathbf{q}(\mathbf{r})] \propto \mathcal{R}e \sum_{\mathbf{k}_p,\lambda} \mathcal{E}_{m\lambda}^*(\mathbf{k}_p)\, \mathcal{A}_{m\lambda}(\mathbf{k}_p) \times \langle \sigma[\mathbf{q}(\mathbf{r}),0]\rangle e^{-i\mathbf{q}(\mathbf{r})\cdot\mathbf{r}} \tag{4}$$

where the abbreviated wavector $\mathbf{q}(\mathbf{r}) \equiv \mathbf{q}_{\{\mathbf{k}\}}(\mathbf{r}) = \mathbf{k}_p - k_p\hat{\mathbf{r}}$, $\mathcal{E}_{m\lambda}(\mathbf{k}_p)$, and $\mathcal{A}_{m\lambda}(\mathbf{k}_p)$ are defined in eqs S9 and S10, respectively. Note that, unlike the coherent or the single photon initial states, the N-photon Fock state signal depends solely on the pump momentum and carries no temporal

DOI: 10.1021/acs.jpclett.9b00071
J. Phys. Chem. Lett. 2019, 10, 768−773

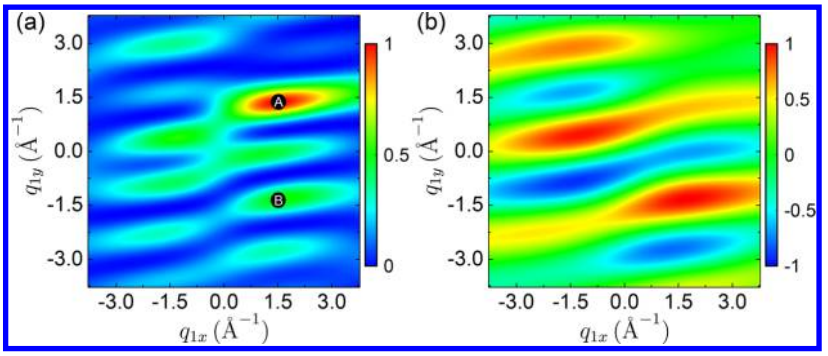

Figure 2. (a) Classical homodyne and (b) first-order linear quantum diffraction $\mathbf{q}_1$ scattering pattern in the q_{1z} = 1.89 Å^{-1} plane. The first pulse $\mathbf{k}_{p1}$ propagates along z. Points A and B were used in the calculated diffraction signals and corresponding time-dependent charge density in Figure 4.

information, since the frequency argument in the charge density is zero. This can be explained as follows: The N-photon Fock state has a fixed number of photons in each mode. Thus, annihilation and consequent creation of the photon must occur in the same mode to conserve the photon number. In contrast, annihilation of the photon in the single-photon Fock state yields the vacuum state. Thus, the diffracted photon created from the vacuum may have a different momentum. The coherent source has a well-defined average photon number, rather than a fixed photon number, which allows diffraction into a mode other than the pump. Similarly the time-resolved equivalent of eq 4 yields

$$S_m^{(1)}[\mathbf{q}(\mathbf{r}),T] \propto \mathcal{R}e \sum_{\mathbf{k}_p,\lambda} \sum_{a,b} \mathcal{E}^*_{m\lambda}(\mathbf{k}_p)\, \mathcal{A}_{m\lambda}(\mathbf{k}_p) \times \mathrm{Tr}\{\sigma_{ab}[\mathbf{q}(\mathbf{r}),0],0)\rho_{ab}^{(0)}(T)\} e^{-i\mathbf{q}(\mathbf{r})\cdot\mathbf{r}+i\phi_{ab}} \quad (5)$$

Heterodyne detection with a classical local oscillator field measures the interference of a noninteracting local oscillator with interacting beam (see eq S12). The role of the local oscillator is then played by vacuum field fluctuations, which is coupled to modes scattered off the matter.

Multidimensional Quantum Diffraction. Spontaneous fluctuations of any physical quantity are described by its multipoint correlation functions. In the case of the charge density, these are $\langle \sigma(\mathbf{q}_1,T_1)\, \sigma(\mathbf{q}_2,T_2) \cdots \rangle$. We now show how these can be measured by a series of quantum diffraction processes. We consider a single molecule undergoing a sequence of[26] n quantum diffraction events. The pulses can have arbitrary spectral and temporal profiles, provided they are temporally well-separated and tuned far from any material resonance. An nth order coincidence counting of LQD photons at positions ($\mathbf{r}_1$, $\mathbf{r}_2$, ..., $\mathbf{r}_n$) is generated by multiple incoming single photon pulses with momenta ($\mathbf{k}_{p1}$, $\mathbf{k}_{p2}$, ..., $\mathbf{k}_{pn}$) and delays (T_1, T_2, ..., T_n).

$$S_q^{(n)}(\mathbf{q}_1,T_1;\ldots;\mathbf{q}_n,T_n) \propto \mathcal{E}_1 \ldots \mathcal{E}_n \times \langle \mathcal{T}\bar{\sigma}(\mathbf{q}_1,T_1) \ldots \bar{\sigma}(\mathbf{q}_n,T_n)\rangle \quad (6)$$

where $\bar{\sigma} = \sigma + \sigma^\dagger$, and the first momentum transfer is $\mathbf{q}_1 = \mathbf{k}_{p1} - \mathbf{k}_1$, followed by $\mathbf{q}_2 = \mathbf{k}_{p2} - \mathbf{k}_2$, etc., with $\mathbf{k}_n$ being the wavevector of the scattered photon.

We now examine the two lowest-order signals. In the simplest (2D) experiment, the molecule is subjected to two off-resonant pulses, with wavevectors $\mathbf{k}_{p1}$ and $\mathbf{k}_{p2}$. A scattered single-photon amplitude from pulse 1 with frequency ω_1 is contracted with the incoming photon amplitude, and the diffracted photon is collected in the direction $\mathbf{k}_1$ at time T_1. The molecule is in a superposition state during the interpulse delay, after which the second pulse is scattered, and the photon amplitude is contracted with the incoming photon amplitude such that the diffracted photon with frequency ω_2 is collected in the $\mathbf{k}_2$ direction at time T_2.

In the impulsive limit, the 2D signal can be written as (see Figure S1 of the Supporting Information and discussion therein)

$$S^{(2)}(\mathbf{q}_1,T_1;\mathbf{q}_2,T_2) \propto \langle \bar{\sigma}(\mathbf{q}_2,T_2)\, \bar{\sigma}(\mathbf{q}_1,T_1)\rangle \quad (7)$$

Higher-order signals can be calculated similarly.

We have simulated the 2D diffraction signals (eq 7) from a single oriented cysteine molecule (see Figure 1b,c). Quantum chemistry calculations were performed by using the MOLPRO code.[27] The optimized geometry was obtained at the Hartree–Fock/cc-pVDZ[28] level of theory. The lowest six valence electronic energy levels were calculated at the CASSCF(6/6)/cc-pVDZ level of theory[29−31] are depicted in Figure 1d. The transition density matrix was evaluated using

$$\sigma_{ij}(\mathbf{r}) = \sum_{mn} T_{mn}^{(ij)} \phi_m(\mathbf{r})\, \phi_n(\mathbf{r}) \quad (8)$$

Here, the indices i, j run over the valence eigenstates. $T_{mn}^{(ij)}$ is the transition density-matrix element between states i and j for the m and n atomic orbitals.

We consider diffraction signals from the ground state (g). In the impulsive limit, the classical homodyne signal for single pulse scattering is given by the sum-over-states expression eq S16, which determines the (transition) charge density in momentum space $\sigma_{ag}(\mathbf{q}_1)$ between two electronic states a and g and diffracted momentum is $\mathbf{q}_1 \equiv \mathbf{k}_1 - \mathbf{k}_{p1}$. The homodyne detected signal eq S16 misses the phase of $\sigma_{ag}(\mathbf{q}_1)$.

The linear (1D) quantum diffraction signal solely gives the ground state charge density:

$$S_q^{(1)}(\mathbf{q}_1,T_1) \propto \langle \bar{\sigma}(\mathbf{q}_1,T_1)\rangle = 2\mathcal{R}e[\sigma_{gg}(\mathbf{q}_1,T_1)] \quad (9)$$

Both signals eqs S16 and 9 are independent of the time delay T_1. Time-dependent signals can be obtained by first preparing the molecule in a superposition state.[18,23] The first pulse $\mathbf{k}_{p1}$ propagates along z, while the $\mathbf{q}_1$ diffraction signals $S_c^{(2)}(\mathbf{q}_1)$ and $S_q^{(1)}(\mathbf{q}_1)$ are detected in the (q_{1x}, q_{1y}) plane; see Figure 2. The scattering shows a rich pattern in $\mathbf{q}_1$ space. The homodyne detected signal (Figure 2a) is positive, and several peaks can be observed in the $\mathbf{q}_1$ domain. The linear quantum diffraction signal may be negative. The classical $S_c^{(2)}$ signal (eq S16) is expressed as the modulus square form of (transition) charge densities in momentum space. The quantum $S_q^{(1)}$ signal (eq 9)

DOI: 10.1021/acs.jpclett.9b00071
J. Phys. Chem. Lett. 2019, 10, 768−773

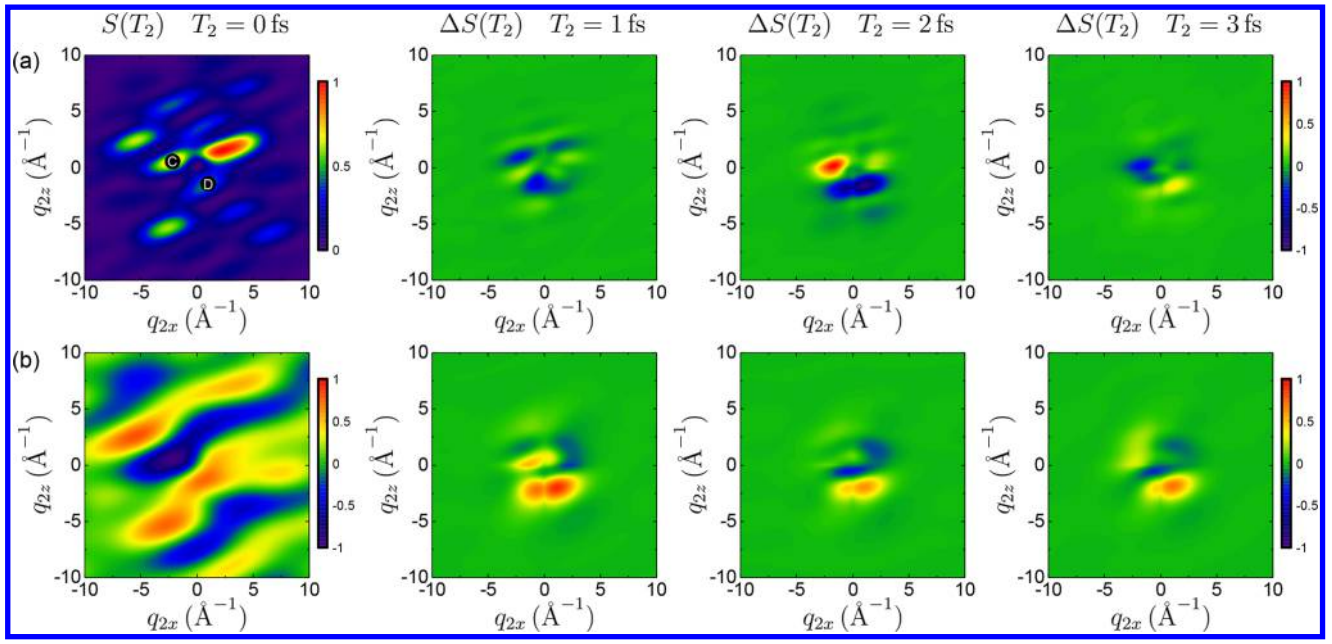

Figure 3. $\mathbf{q}_2$ diffraction patterns at the given $\mathbf{q}_1$ point A for (a) classical homodyne $S_c^{(4)}(\mathbf{q}_1,T_1{=}0;\mathbf{q}_2,T_2)$ and (b) second-order linear quantum diffraction $S_q^{(2)}(\mathbf{q}_1,T_1{=}0;\mathbf{q}_2,T_2)$ signals at four time delays T_2 in the $q_{2y} = 1.89$ Å^{-1} plane. The second pulse $\mathbf{k}_{p2}$ propagates along y. To highlight the changes, in columns 2, 3, and 4, we plot the signal difference $\Delta S(T_2) = S(T_2) - S(T_2 = 0)$.

in contrast depends on both the amplitude and phase of charge densities, making it possible to extract the real space ground state charge density $\sigma_{gg}(\mathbf{r})$.

To study the charge density dynamical fluctuations, we resort to the $S_q^{(2)}$ signal. To investigate the two-photon coincidence scattering pattern in $\mathbf{q}_2$ space, we select the $\mathbf{q}_1$ point A = (1.51 Å^{-1}, 1.36 Å^{-1}) in Figure 2a. The classical homodyne signal for $\mathbf{q}_2$ scattering is given by eq S18. The second-order LQD signal is

$$S_q^{(2)}(\mathbf{q}_1,T_1{=}0;\mathbf{q}_2,T_2) \propto \langle \bar{\sigma}(\mathbf{q}_2,T_2)\,\bar{\sigma}(\mathbf{q}_1,0)\rangle = \sum_a [\sigma_{ga}(\mathbf{q}_2) + \sigma_{ag}^*(\mathbf{q}_2)][\sigma_{ag}(\mathbf{q}_1) + \sigma_{ga}^*(\mathbf{q}_1)]e^{-i\omega_{ag}T_2} \quad (10)$$

Because the molecule is initially in the ground state, the signal depends only on the second time delay T_2.

Figure 3 depicts the $\mathbf{q}_2$ scattering pattern in the $q_{2y} = 1.89$ Å^{-1} plane, where the second pulse $\mathbf{k}_{p2}$ propagates along y. The first column shows the signals at $T_2 = 0$. Again, we see that the classical $S_c^{(4)}$ signal (Figure 3a) is always positive, while the quantum signal $S_q^{(2)}$ (Figure 3b) may be negative. Since signal is dominated by the time-independent pathways, i.e., c = d in eq S18 and a = g in eq 10, the diffraction signals at different time delays look very similar. To better visulize the changes, we plot the signal difference $S(T_2) - S(T_2{=}0)$ in columns 2, 3, and 4, where the time-independent background has been subtracted. Rich temporal patterns in $\mathbf{q}_2$ originate from interferences between the various scattering pathways. By Fourier transform of the time-domain signal into the frequency (Ω) domain, we can identify the electronic coherences that contribute to the dynamics of the signal. In Figure S2 of the Supporting Information we display such spectra at the points C and D of Figure 3.

The classical $S_c^{(4)}$ signal represents the electron density fluctuations in momentum space and may be used to image the real-space charge-density correlation functions. The quantum-phase-dependent $S_q^{(2)}$ signal, in contrast, can retrieve the time-dependent transition charge densities in real space. Fourier transformation of the second-order LQD signal eq 10 into real space $\mathbf{r}_2$ at a given $\mathbf{q}_1$ point in Figure 2 gives

$$S_q^{(2)}(\mathbf{q}_1,T_1{=}0;\mathbf{r}_2,T_2) \propto \int d\mathbf{q}_2\, e^{i\mathbf{q}_2\cdot\mathbf{r}_2} S_q^{(2)}(\mathbf{q}_1,T_1{=}0;\mathbf{q}_2,T_2) = 2\sum_a [\sigma_{ag}(\mathbf{q}_1) + \sigma_{ga}^*(\mathbf{q}_1)]e^{-i\omega_{ag}T_2}\sigma_{ga}(\mathbf{r}_2) \quad (11)$$

Figure 4 depicts the real-space signal at the two $\mathbf{q}_1$ points A and B marked in Figure 2 for different time delays T_2. At $T_2 = 0$ fs, the signal looks similar to the ground state charge density (see Figure 1c), because the $\sigma_{gg}(\mathbf{r}_2)$ term dominates eq 4. As in Figure 3 the other plots at $T_2 \neq 0$ have this signal subtracted, and thus image the dynamics of transition charge densities in real space. For points A and B in Figure 2, the real-space signals show a very different time dependence, because different momenta $\mathbf{q}_1$ are transferred to the electrons by the first pulse $\mathbf{k}_{p1}$. The spatial Fourier-transformed real-space signal eq 11 is a combination of various (transition) charge densities $\sigma_{ga}(\mathbf{r})$ and can provide information about quantum coherence between the ground and excited states.

To compare the LQD signals (eq 5) with classical diffraction,[32] we first note that the former vanishes for a classical field and requires a quantum field. Furthermore, using a light source in which the quantum nature of radiation is prominent, the signal reveals both the amplitude and phase of the charge density. The diffraction can originate from a group of molecules initially in their ground states with a small fraction in the excited state. The relevant material quantity in eq S15 is then $\langle\sigma_{gg}\rangle_\alpha\langle\sigma_{ag}\rangle_\beta$ where α and β represent two molecules, σ_{ag} is a transition charge density (coherence). Classical homodyne diffraction is quadratic in the charge density and originates from pairs of molecules (see section S2 of the Supporting Information). The single-molecule contribution, in contrast, originates solely from excited state population since the trace

DOI: 10.1021/acs.jpclett.9b00071
J. Phys. Chem. Lett. 2019, 10, 768−773

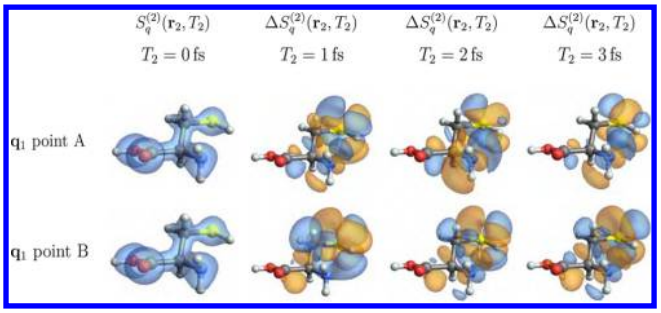

Figure 4. Time-dependent charge density obtained using eq 11 for $\mathbf{q}_1$ points A = (1.51 Å^{-1}, 1.36 Å^{-1}) and B = (+1.51 Å^{-1}, −1.36 Å^{-1}) marked in Figure 2. We show the full signal at $T_2 = 0$ fs, and the signal differences $\Delta S_q^{(2)}(\mathbf{r}_2,T_2) = S_q^{(2)}(\mathbf{q}_1,T_1{=}0;\mathbf{r}_2,T_2) - S_q^{(2)}(\mathbf{q}_1,T_1{=}0;\mathbf{r}_2,T_2{=}0)$ for other plots.

of the diffracted field operators in the expectation value with respect to vacuum state of the field vanishes if the molecule is in a coherent superposition. Classical diffraction carries no information about single molecule coherence.

The multidimensional extension of diffraction imaging with classical light to n diffraction events scales to nth order in the light *intensity* and 2nth order in the charge density (see section S2 of the Supporting Information). The corresponding quantum light signal presented here, in contrast, scales to nth order in the field *amplitude*. Thus, at a given intensity quantum light allows to observe higher-order correlations, thanks to the more favorable intensity scaling. Classical homodyne diffraction dominated by even orders in the charge density is governed by the static (localized) charge density while the new information carried by the phase in the odd order contributions provides a novel way of measuring transient charge density, density−density correlations and dynamical events in molecules using quantum diffraction. Generally, the nth order signals have both amplitude square contributions and lower-order phase-dependent contributions (such as the ones explored in Figure 1). For intense quantum sources with many photons the contribution quadratic in the charge density dominates and the phase-dependent terms merely provide a minor correction to the strong background. It is therefore critical to use low photon fluxes in order to isolate the phase-dependent contributions. An alternative way to single out these terms is by employing multiple single photon interferences generated by introducing beam splitters in, e.g., Mach−Zehnder interferometers (MZI). The phase of the classical local oscillator field allows us to separate real and imaginary parts of the material response function and extract the phase in heterodyne measurement. Similar results can be obtained for quantum field by combining the MZI with the phase plates. The multidimensional analogue will be an interesting topic for a future study.

■ ASSOCIATED CONTENT

Supporting Information

The Supporting Information is available free of charge on the ACS Publications website at DOI: 10.1021/acs.jpclett.9b00071.

Details of the LQD signal derivation, classical 1D and 2D homodyne and heterodyne diffraction signals, and simulations of real and imaginary parts of frequency domain quantum and classical signals (PDF)

■ AUTHOR INFORMATION

Corresponding Authors

*E-mail: dorfmank@lps.ecnu.edu.cn.
*E-mail: sasban@uci.edu.
*E-mail: smukamel@uci.edu.

ORCID

Konstantin E. Dorfman: 0000-0001-9963-0878
Jérémy R. Rouxel: 0000-0003-3438-6370
Daeheum Cho: 0000-0002-0322-4291
Shaul Mukamel: 0000-0002-6015-3135

Notes

The authors declare no competing financial interest.

■ ACKNOWLEDGMENTS

K.E.D. is supported by the Zijiang Endowed Young Scholar Fund, East China Normal University and Overseas Expertise Introduction Project for Discipline Innovation (111 Project, B12024). S.M. acknowledges the National Science Foundation (grant CHE-1663822) and the support of the Chemical Sciences, Geosciences, and Biosciences division, Office of Basic Energy Sciences, Office of Science, U.S. Department of Energy, through award No. DE-FG02-04ER15571 and DE-SC0019484. S.A. was supported by the DOE grant. We wish to thank Noa Asban for the graphical illustrations.

■ REFERENCES

(1) Glauber, R. J. The Quantum Theory of Optical Coherence. *Phys. Rev.* **1963**, *130*, 2529−2539.
(2) Hong, C.-K.; Ou, Z.-Y.; Mandel, L. Measurement of subpicosecond time intervals between two photons by interference. *Phys. Rev. Lett.* **1987**, *59*, 2044.
(3) Branning, D.; Migdall, A. L.; Sergienko, A. Simultaneous measurement of group and phase delay between two photons. *Phys. Rev. A: At., Mol., Opt. Phys.* **2000**, *62*, 063808.
(4) Trotta, R.; Martín-Sánchez, J.; Wildmann, J. S.; Piredda, G.; Reindl, M.; Schimpf, C.; Zallo, E.; Stroj, S.; Edlinger, J.; Rastelli, A. Wavelength-tunable sources of entangled photons interfaced with atomic vapours. *Nat. Commun.* **2016**, *7*, 10375.
(5) Kalashnikov, D. A.; Paterova, A. V.; Kulik, S. P.; Krivitsky, L. A. Infrared spectroscopy with visible light. *Nat. Photonics* **2016**, *10*, 98.
(6) Lee, J.-C.; Kim, Y.-H. Spatial and spectral properties of entangled photons from spontaneous parametric down-conversion with a focused pump. *Opt. Commun.* **2016**, *366*, 442−450.
(7) Nordén, B. Entangled photons from single atoms and molecules. *Chem. Phys.* **2018**, *507*, 28−33.
(8) Paterova, A. V.; Yang, H.; An, C.; Kalashnikov, D. A.; Krivitsky, L. A. Tunable optical coherence tomography in the infrared range using visible photons. *Quant. Sci. and Technol.* **2018**, *3*, 025008.
(9) Krausz, F.; Ivanov, M. Attosecond physics. *Rev. Mod. Phys.* **2009**, *81*, 163.
(10) Ishikawa, T.; Aoyagi, H.; Asaka, T.; Asano, Y.; Azumi, N.; Bizen, T.; Ego, H.; Fukami, K.; Fukui, T.; Furukawa, Y.; et al. A compact X-ray free-electron laser emitting in the sub-ångström region. *Nat. Photonics* **2012**, *6*, 540.
(11) Corde, S.; Phuoc, K. T.; Lambert, G.; Fitour, R.; Malka, V.; Rousse, A.; Beck, A.; Lefebvre, E. Femtosecond x rays from laser-plasma accelerators. *Rev. Mod. Phys.* **2013**, *85*, 1.
(12) Chini, M.; Zhao, K.; Chang, Z. The generation, characterization and applications of broadband isolated attosecond pulses. *Nat. Photonics* **2014**, *8*, 178.
(13) Bostedt, C.; Boutet, S.; Fritz, D. M.; Huang, Z.; Lee, H. J.; Lemke, H. T.; Robert, A.; Schlotter, W. F.; Turner, J. J.; Williams, G. J. Linac coherent light source: The first five years. *Rev. Mod. Phys.* **2016**, *88*, 015007.

DOI: 10.1021/acs.jpclett.9b00071
J. Phys. Chem. Lett. 2019, 10, 768−773

(14) Cohen, A. E.; Mukamel, S. Resonant Enhancement and Dissipation in Nonequilibrium van der Waals Forces. *Phys. Rev. Lett.* **2003**, *91*, 233202.
(15) Mukamel, S.; Dorfman, K. E. Nonlinear fluctuations and dissipation in matter revealed by quantum light. *Phys. Rev. A: At., Mol., Opt. Phys.* **2015**, *91*, 053844.
(16) Miao, J.; Charalambous, P.; Kirz, J.; Sayre, D. Extending the methodology of X-ray crystallography to allow imaging of micrometre-sized non-crystalline specimens. *Nature* **1999**, *400*, 342.
(17) Miao, J.; Ishikawa, T.; Anderson, E. H.; Hodgson, K. O. Phase retrieval of diffraction patterns from noncrystalline samples using the oversampling method. *Phys. Rev. B: Condens. Matter Mater. Phys.* **2003**, *67*, 174104.
(18) Rouxel, J. R.; Kowalewski, M.; Bennett, K.; Mukamel, S. X-Ray Sum Frequency Diffraction for Direct Imaging of Ultrafast Electron Dynamics. *Phys. Rev. Lett.* **2018**, *120*, 243902.
(19) Marx, C. A.; Harbola, U.; Mukamel, S. Nonlinear optical spectroscopy of single, few, and many molecules: Nonequilibrium Green's function QED approach. *Phys. Rev. A: At., Mol., Opt. Phys.* **2008**, *77*, 022110.
(20) Maiden, A. M.; Rodenburg, J. M. An improved ptychographical phase retrieval algorithm for diffractive imaging. *Ultramicroscopy* **2009**, *109*, 1256−1262.
(21) Candès, E.; Eldar, Y.; Strohmer, T.; Voroninski, V. Phase Retrieval via Matrix Completion. *SIAM Rev.* **2015**, *57*, 225−251.
(22) Asban, S.; Dorfman, K. E.; Mukamel, S. Enhanced resolution microscopy using light-entanglement and quantum unraveling. Unpublished.
(23) Bennett, K.; Biggs, J. D.; Zhang, Y.; Dorfman, K. E.; Mukamel, S. Time-, frequency-, and wavevector-resolved x-ray diffraction from single molecules. *J. Chem. Phys.* **2014**, *140*, 204311.
(24) Tanaka, S.; Chernyak, V.; Mukamel, S. Time-resolved X-ray spectroscopies: Nonlinear response functions and Liouville-space pathways. *Phys. Rev. A: At., Mol., Opt. Phys.* **2001**, *63*, 063405.
(25) Chernyak, V. Y.; Saurabh, P.; Mukamel, S. Non-linear non-local molecular electrodynamics with nano-optical fields. *J. Chem. Phys.* **2015**, *143*, 164107.
(26) Mukamel, S.; Bakker, H. J. Special topic on multidimensional spectroscopy. *J. Chem. Phys.* **2015**, *142*, 212101.
(27) Werner, H.; Knowles, P.; Knizia, G.; Manby, F.; Schütz, M.; Celani, P.; Korona, T.; Lindh, R.; Mitrushenkov, A.; Rauhut, G.; et al. *MOLPRO*, version 2010.1, a package of ab initio programs, 2010, see http://www.molpro.net.
(28) Dunning, T. H., Jr Gaussian basis sets for use in correlated molecular calculations. I. The atoms boron through neon and hydrogen. *J. Chem. Phys.* **1989**, *90*, 1007−1023.
(29) Werner, H.-J.; Meyer, W. A quadratically convergent multiconfiguration−self-consistent field method with simultaneous optimization of orbitals and CI coefficients. *J. Chem. Phys.* **1980**, *73*, 2342−2356.
(30) Werner, H.-J.; Knowles, P. J. A second order multiconfiguration SCF procedure with optimum convergence. *J. Chem. Phys.* **1985**, *82*, 5053−5063.
(31) Knowles, P. J.; Werner, H.-J. An efficient second-order MC SCF method for long configuration expansions. *Chem. Phys. Lett.* **1985**, *115*, 259−267.
(32) Kowalewski, M.; Bennett, K.; Mukamel, S. Monitoring nonadiabatic avoided crossing dynamics in molecules by ultrafast X-ray diffraction. *Struct. Dyn.* **2017**, *4*, 054101.

DOI: 10.1021/acs.jpclett.9b00071
J. Phys. Chem. Lett. 2019, 10, 768−773

SUPPLEMENTARY INFORMATION:

Monitoring Spontaneous Charge-density Fluctuations by Single-molecule Diffraction of Quantum Light

Konstantin E. Dorfman,[*,†] Shahaf Asban,[*,‡] Lyuzhou Ye,[‡] Jérémy R. Rouxel,[¶] Daeheum Cho,[‡] and Shaul Mukamel[*,‡]

†*State Key Laboratory of Precision Spectroscopy, East China Normal University, Shanghai 200062, China*

‡*Department of Chemistry and Department of Physics and Astronomy, University of California, Irvine, California 92697-2025, USA*

¶*Laboratory of Ultrafast Spectroscopy, École Polytechnique Fédérale de Lausanne, CH-1015 Lausanne, Switzerland*

§*SwissFEL, Paul Scherrer Institut, 5232 Villigen PSI, Switzerland*

E-mail: Email:dorfmank@lps.ecnu.edu.cn; sasban@uci.edu; smukamel@uci.edu

S1 Derivation of the LQD signal

The diffraction pattern is obtained from the time-integrated spatially-gated intensity at point $\mathbf{r}$ of the detector.

$$S_m\left[\mathbf{q}\left(\mathbf{r}\right)\right] = \int dt F_t^I(\bar{t},t) \\ \times \left\langle \mathcal{T}\mathbf{E}_m^{(-)}\left(\mathbf{r},t\right)\mathbf{E}_m^{(+)}\left(\mathbf{r},t\right)e^{-\frac{i}{\hbar}\int_{-\infty}^{t}d\tau\mathcal{H}_{I-}(\tau)}\right\rangle, \tag{S1}$$

where m is cartesian component of the field, $\mathbf{q}\left(\mathbf{r}\right)$ is the diffraction wavevector corresponing to detection at point $\mathbf{r}$, $F_t^I(\bar{t},t)$ is a temporal gate, and $\mathcal{T}$ is the time ordering superoperator. $\mathcal{H}_{I-}$ is the interaction superoperator, defined by its action on an ordinary operator X according to $\mathcal{H}_{I-}X \equiv \mathcal{H}_I X - X\mathcal{H}_I$ [1]. By expanding the exponent to first order in $\mathcal{H}_{I-}$, and separating the incoming (pump) from the detected modes of the electric field we obtain the LQD signal (see Eq. (S2)). For brevity we assume a temporal gating $F_t^I(\bar{t},t)$ that acts on the intensity, rather than the field (which was $F_t(\bar{t},t)$). The first order expansion of Eq. (S1) in field-matter interaction yields:

$$S_m^{(1)}(\mathbf{r}) = \frac{2}{\hbar}\mathfrak{Im}\int dt F_t^I(\bar{t},t)\int_{-\infty}^{t}dt'\int d\mathbf{r}'\langle\sigma(\mathbf{r}',t')\rangle_\mu \\ \times\sum_n \langle\psi_p(0)|\mathbf{E}_m^{(-)}(\mathbf{r},t)\mathbf{A}_n^{(+)}(\mathbf{r}',t')|\psi_p(0)\rangle\langle 0|\mathbf{E}_m^{(+)}(\mathbf{r},t)\mathbf{A}_n^{(-)}(\mathbf{r}',t')|0\rangle, \tag{S2}$$

where $\mathfrak{Im}$ denotes imaginary part, n represents the cartesian coordinates of the vector potential coming from $\mathbf{A}^2$ interaction term and $\langle ...\rangle_\mu \equiv \mathrm{Tr}[...\rho_\mu^{(0)}]$ is taken with respect to the initial state of the molecule $\rho_\mu^{(0)}$, and $\psi_p(0)$ is the state of the pump photon source.

While the second correlation function over the vacuum state representing detection modes is the same as in the field amplitude signal, the first correlation function over the pump photon state is more peculiar. Assuming the coherent state, the field correlation function

reads

$$\langle\psi_p(0)|\mathbf{E}_m^{(-)}(\mathbf{r},t)\mathbf{A}_n^{(+)}(\mathbf{r}',t')|\psi_p(0)\rangle = \mathcal{E}_m^*(\mathbf{r},t)\mathcal{A}_n(\mathbf{r}',t'), \tag{S3}$$

where $\mathcal{E}_m(\mathbf{r},t) = \sum_{\mathbf{k},\mu}\sqrt{\frac{2\pi\hbar\omega_\mathbf{k}}{V_\mathbf{k}}}\epsilon_m^{(\mu)}(\mathbf{k})\alpha_{\mathbf{k},\mu}e^{i(\mathbf{k}\cdot\mathbf{r}-\omega_\mathbf{k}t)}$ and $\mathcal{A}_n(\mathbf{r},t) = -ic\sum_{\mathbf{k},\mu}\sqrt{\frac{2\pi\hbar}{\omega_\mathbf{k}V_\mathbf{k}}}\epsilon_m^{(\mu)}(\mathbf{k})\alpha_{\mathbf{k},\mu}e^{i(\mathbf{k}\cdot\mathbf{r}-\omega_\mathbf{k}t)}$ with $\alpha_{\mathbf{k},\mu} = \langle\alpha|\hat{a}_{\mathbf{k},\mu}|\alpha\rangle$. Note that a similar expression can be achieved for a single photon Fock state $|\psi_{1F}(0)\rangle = \sum_{\mathbf{p},\lambda}\Phi_{\mathbf{p},\lambda}|1_{\mathbf{p},\lambda}\rangle$. In this case the corresponding field amplitudes are given by $\mathcal{E}_m(\mathbf{r},t) = \sum_{\mathbf{k},\mu}\sqrt{\frac{2\pi\hbar\omega_\mathbf{k}}{V_\mathbf{k}}}\epsilon_m^{(\mu)}(\mathbf{k})\Phi_{\mathbf{k},\mu}e^{i(\mathbf{k}\cdot\mathbf{r}-\omega_\mathbf{k}t)}$ and $\mathcal{A}_n(\mathbf{r},t) = -ic\sum_{\mathbf{k},\mu}\sqrt{\frac{2\pi\hbar}{\omega_\mathbf{k}V_\mathbf{k}}}\epsilon_m^{(\mu)}(\mathbf{k})\Phi_{\mathbf{k},\mu}e^{i(\mathbf{k}\cdot\mathbf{r}-\omega_\mathbf{k}t)}$ with $\Phi_{\mathbf{k},\mu} = \langle 0|\hat{a}_{\mathbf{k},\mu}|\psi_{1F}(0)\rangle$. Following the method outlined previously and using the following identity:

$$\begin{aligned}&\frac{2\pi\hbar}{V_\mathbf{k}}\sum_\mathbf{k}\epsilon_m^{(\mu)}(\mathbf{k})\epsilon_n^{(\mu)}(\mathbf{k})e^{i\mathbf{k}\cdot\mathbf{R}}\int_{-\infty}^{t}dt'e^{-i\omega_\mathbf{k}(t-t')-i\Omega t'} = \\ &\frac{\hbar}{4\pi}\left[\frac{\Omega^2}{c^2}(\delta_{m,n}-\hat{\mathbf{r}}_m\hat{\mathbf{r}}_n)+\left(\frac{i\Omega}{cR}-\frac{1}{R^2}\right)(\delta_{m,n}-3\hat{\mathbf{r}}_m\hat{\mathbf{r}}_n)\right]\frac{e^{-i\Omega(t-R/c)}}{\Omega R}\end{aligned} \tag{S4}$$

we obtain for the signal

$$\begin{aligned}S_m^{(1)}(\mathbf{r}) \propto \mathfrak{Re}\int\frac{d\omega'}{2\pi}\sum_{\mathbf{k},\mathbf{k}_p}\tilde{F}_t^I(\bar{t},\omega'-\omega_{\mathbf{k}_p}+\omega_\mathbf{k})\langle\sigma(\mathbf{q}_r(\omega'),\omega')\rangle\sum_n\mathcal{E}_m^*(\mathbf{k})\mathcal{A}_n(\mathbf{k}_p) \\ \times\left[\frac{\omega_{\mathbf{k}_p}-\omega'}{c}(\delta_{m,n}-\hat{\mathbf{r}}_m\hat{\mathbf{r}}_n)+\frac{i}{r}(\delta_{m,n}-3\hat{\mathbf{r}}_m\hat{\mathbf{r}}_n)\right]e^{i(\omega_{\mathbf{k}_p}-\omega')r/c-i\mathbf{k}\cdot\mathbf{r}}\end{aligned} \tag{S5}$$

where $\tilde{F}_t^I(\bar{t},\omega) = \int dt e^{i\omega t}F_t^I(\bar{t},t)$ is a Fourier transform of the gating function,

$$\mathcal{E}_m^*(\mathbf{k}) = \sum_\mu\sqrt{\frac{2\pi\hbar\omega_\mathbf{k}}{V_\mathbf{k}}}\epsilon_m^{(\mu)}(\mathbf{k})\chi_{\mathbf{k},\mu}, \tag{S6}$$

$$\mathcal{A}_n(\mathbf{k}_p) = -ic\sum_\lambda\sqrt{\frac{2\pi\hbar}{\omega_{\mathbf{k}_p}V_{\mathbf{k}_p}}}\epsilon_n^{(\lambda)}(\mathbf{k}_p)\chi_{\mathbf{k}_p,\lambda}, \tag{S7}$$

where $\chi = \alpha$ for coherent state and $\chi = \Phi$ for single photon Fock state. Now assuming no temporal gate and taking rotating averaging we obtain Eq. (1).

For the N-photon Fock state the field correlation function Eq. (S3) will contain only same momentum and polarization components of the two fields:

$$\langle\psi_p(0)|\mathbf{E}_m^\dagger(\mathbf{r},t)\mathbf{A}_{pn}(\mathbf{r}',t')|\psi_p(0)\rangle = \sum_{\mathbf{k}_p,\lambda}\mathcal{E}_{m\lambda}^*(\mathbf{k}_p)\mathcal{A}_{n\lambda}(\mathbf{k}_p)e^{-i[\mathbf{k}_p(\mathbf{r}-\mathbf{r}')-\omega_{\mathbf{k}_p}(t-t')]}, \tag{S8}$$

where

$$\mathcal{E}_{m\lambda}^*(\mathbf{k}_p) = \sqrt{\frac{2\pi\hbar\omega_{\mathbf{k}_p}N_{\mathbf{k}_p,\lambda}}{V_{\mathbf{k}_p}}}\Phi_{\mathbf{k}_p,\lambda}^{(N)*}\epsilon_m^{(\lambda)}(\mathbf{k}_p), \tag{S9}$$

and

$$\mathcal{A}_{n\lambda}(\mathbf{k}_p) = -ic\sqrt{\frac{2\pi\hbar N_{\mathbf{k}_p,\lambda}}{\omega_{\mathbf{k}_p}V_{\mathbf{k}_p}}}\Phi_{\mathbf{k}_p,\lambda}^{(N)}\epsilon_n^{(\lambda)}(\mathbf{k}_p). \tag{S10}$$

Here we use $\langle\psi_{NF}(0)|\hat{a}_{\mathbf{k},\nu}^\dagger\hat{a}_{\mathbf{k}_p,\lambda}|\psi_{NF}(0)\rangle = N_{\mathbf{k}_p,\lambda}|\Phi_{\mathbf{k}_p,\lambda}^{(N)}|^2\delta_{\mathbf{k},\mathbf{k}_p}\delta_{\nu,\lambda}$. Following the outlined approach the LQD signal yields

$$\begin{aligned} S_m^{(1)}(\mathbf{r}) \propto \mathfrak{Re}\int\frac{d\omega'}{2\pi}\sum_{\mathbf{k}_p,\lambda}\tilde{F}_t^I(\bar{t},\omega')\langle\sigma(\mathbf{q}_r(\omega'),\omega')\rangle\sum_n\mathcal{E}_{m\lambda}^*(\mathbf{k}_p)\mathcal{A}_{n\lambda}(\mathbf{k}_p) \\ \times\left[\frac{\omega_{\mathbf{k}_p}-\omega'}{c}(\delta_{m,n}-\hat{\mathbf{r}}_m\hat{\mathbf{r}}_n)+\frac{i}{r}(\delta_{m,n}-3\hat{\mathbf{r}}_m\hat{\mathbf{r}}_n)\right]e^{i(\omega_{\mathbf{k}_p}-\omega')r/c-i\mathbf{k}_p\cdot\mathbf{r}}, \end{aligned} \tag{S11}$$

where $\mathbf{q}(\mathbf{r}) = \mathbf{k}_p + \frac{\omega'-\omega_p}{c}\hat{\mathbf{r}}$. Assuming no temporal gate and taking rotating averaging we simplify the signal to Eq. (4).

The 2D extension of the LQD signal resulting from the two successive scattering measurements is described by the two diagrams of Fig.($S1$) (and their complex conjugates) stemming from the separation of σ and $\sigma^\dagger$ that correspond either to both scattering events occur with the ket, or with the ket and the bra (see Fig. S1(b)). The complex conjugate diagrams are not shown. The signal can be read off the diagram and is given by Eq. (7).

S2 Diffraction of classical light

S2.1 Heterodyne detection

A classical heterodyne diffraction is measured by mixing classical diffracted field with another classical local oscillator field. The signal is given by

$$S_c(\mathbf{r}) = \frac{2}{\hbar}\mathfrak{Im}\int dt\mathcal{A}_d^*(\mathbf{r},t)\int dt_1 d\mathbf{r}_1\mathcal{A}_p(\mathbf{r}_1,t_1)\langle\sigma(\mathbf{r}_1,t_1)\rangle_\mu \tag{S12}$$

This signal is also linear in the charge density. Following the similar derivation presented in Appendix A we obtain for the signal in the CW limit

$$S_c^{(1)}(\mathbf{r}) \propto \mathfrak{Re}[\mathcal{A}_d^*(\omega_0)\mathcal{A}_p(\omega_0)\langle\sigma\left(\mathbf{q}_\mathbf{r}(0),0\right)\rangle_\mu e^{-i\mathbf{k}_{p'}\cdot\mathbf{r}}]. \tag{S13}$$

S2.2 Homodyne detection

Unlike quantum case and heterodyne classical detection, classical homodyne signal is linear in the field intensity and quadratic in the charge density.

$$\begin{aligned} S_c^{(2)}(\mathbf{r}) = \frac{2}{\hbar^2}\mathfrak{Re}\int dtd\mathbf{r}_1 d\mathbf{r}_1 dt_1 dt_2\langle\sigma\left(\mathbf{r}_2,t_2\right)\sigma\left(\mathbf{r}_1,t_1\right)\rangle_\mu \\ \times\langle\mathbf{A}^2\left(\mathbf{r}_2,t_2\right)\mathbf{E}^{(-)}\left(\mathbf{r},t\right)\mathbf{E}^{(+)}\left(\mathbf{r},t\right)\mathbf{A}^2\left(\mathbf{r}_1,t_1\right)\rangle_\phi. \end{aligned} \tag{S14}$$

Following the same steps discussed above the homodyne signal for CW pump is given by

$$S_c^{(2)}(\mathbf{r}) \propto \langle|\sigma\left(\mathbf{q}_\mathbf{r}(0),0\right)|^2\rangle_\mu. \tag{S15}$$

Assuming no preparation and time-delayed diffraction denoted by T_1 and expanding the

signal Eq. (S15) in sum-over states yields

$$S_c^{(2)}(T_1, \mathbf{q}_1) \propto \left\langle \sigma^\dagger(T_1, \mathbf{q}_1)\sigma(T_1, \mathbf{q}_1)\right\rangle = \sum_a |\sigma_{ag}(\mathbf{q}_1)|^2 . \tag{S16}$$

S2.3 Multidimensional classical diffraction

The signals studied by Biggs et al.[2] employ contributions linear in the field intensities and are analogous to classical signals which in the impulsive limit read

$$\begin{aligned} &S_c^{(2n)}(\mathbf{q}_1, T_1; ...; \mathbf{q}_n, T_n) \propto I_1....I_n \\ &\times \langle\langle \mathcal{T}\sigma^\dagger(T_1, \mathbf{q}_1)\sigma(T_1, \mathbf{q}_1)...\sigma^\dagger(T_n, \mathbf{q}_n)\sigma(T_n, \mathbf{q}_n)\rangle\rangle, \end{aligned} \tag{S17}$$

where $I_j = |\mathcal{E}_j|^2$ are field intensities. In Eq. (S17) each diffraction event is quadratic in σ and we omitted the frequency argument in the charge density. Expanding the $n = 2$ signal in sum-over states yields

$$\begin{aligned} &S_c^{(4)}(T_1 = 0, \mathbf{q}_1, T_2, \mathbf{q}_2) \propto \left\langle \sigma^\dagger(T_1 = 0, \mathbf{q}_1)\sigma^\dagger(T_2, \mathbf{q}_2)\sigma(T_2, \mathbf{q}_2)\sigma(T_1 = 0, \mathbf{q}_1)\right\rangle \\ &= \sum_{ecd} \sigma_{cg}(\mathbf{q}_1)\sigma^*_{dg}(\mathbf{q}_1)\sigma_{ec}(\mathbf{q}_2)\sigma^*_{ed}(\mathbf{q}_2)e^{-i\omega_{cd}T_2}. \end{aligned} \tag{S18}$$

S3 The classical homodyne and LQD signals in frequency domain

We select two points C = $(-2.17\,\text{Å}^{-1}, 0.47\,\text{Å}^{-1})$ and D = $(0.95\,\text{Å}^{-1}, -1.42\,\text{Å}^{-1})$ in Fig. 3(a), and depict the frequency-domain signals in Fig. S2. The peaks at $\Omega = 0$, which correspond to the time-independent pathways and overwhelm other peaks away from the origin ($\Omega = 0$), have been excluded from Fig. S2. We conclude that the time dependence of the signal is determined by the energy differences between the ground and the excited states.

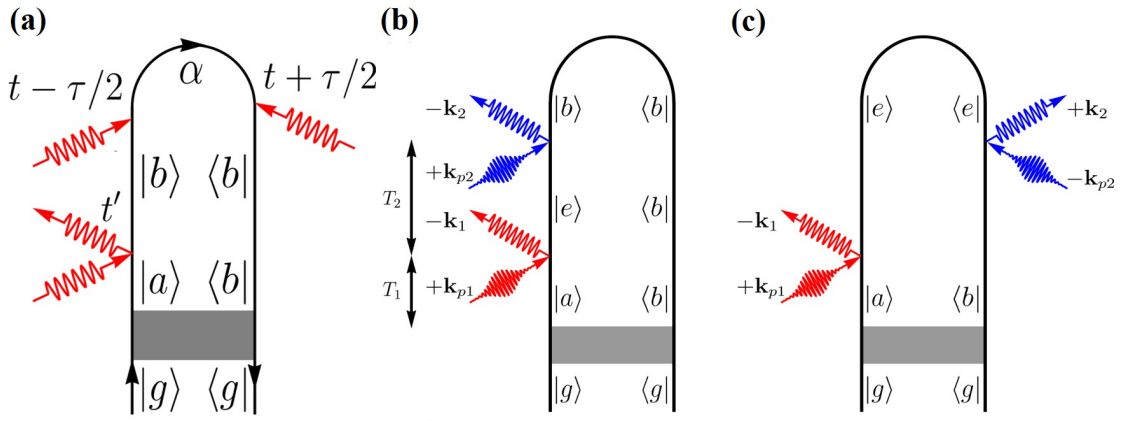

Figure S1: (a) The loop diagram for the LQD process. An actinic pulse (shaded area) prepares the molecule in a superposition of electronic states ρ_{ab}. After the LQD the state of the system is ρ_{bb}. The top two arrows represent the detection.(b) and (c) The loop diagrams representing the LQD signal in Eq. (7) resulting from two successive scattering measurements. For diagram rules see Ref.[3]

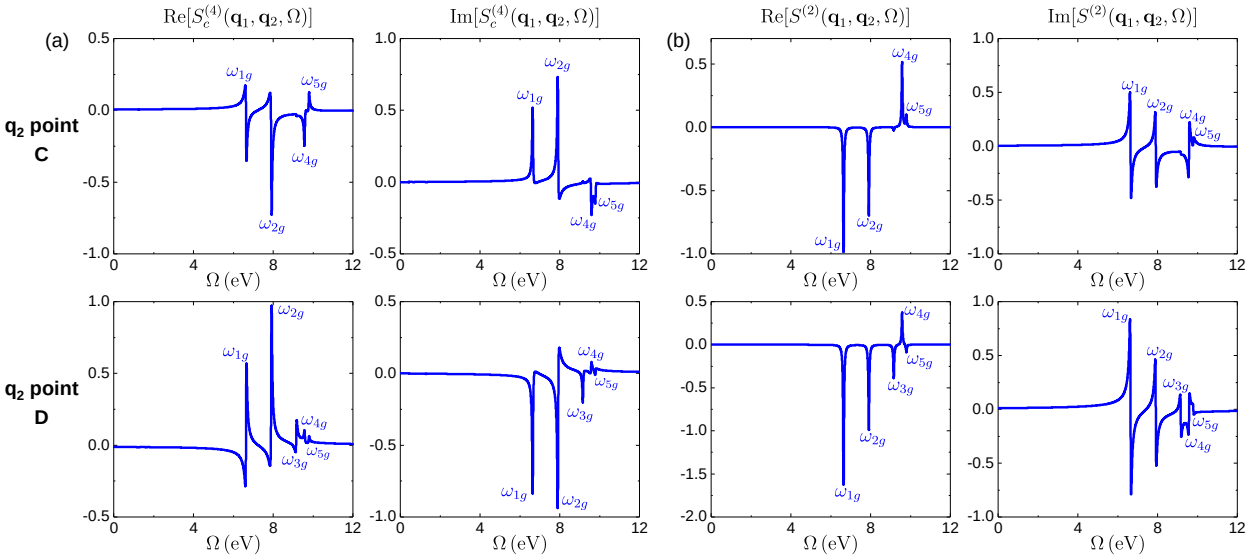

Figure S2: The real and imaginary parts of signals for (a) classical homodyne $S_c^{(4)}(\mathbf{q}_1,\mathbf{q}_2,\Omega)$ (columns 1 and 2) and (b) LQD $S_q^{(2)}(\mathbf{q}_1,\mathbf{q}_2,\Omega)$ (columns 3 and 4) in frequency domain. The first and second rows show signals at the $\mathbf{q}_2$ points C and D marked in Fig. 3(a), respectively.

References

(1) Harbola, U.; Mukamel, S. *Phys. Rep.* **2008**, *465*, 191.

(2) Biggs, J. D.; Bennett, K.; Zhang, Y.; Mukamel, S. Multidimensional scattering of attosecond x-ray pulses detected by photon-coincidence. *J. Phys. B: At. Mol. Opt. Phys.* **2014**, *47*, 124037.

(3) Marx, C. A.; Harbola, U.; Mukamel, S. Nonlinear optical spectroscopy of single, few, and many molecules: Nonequilibrium Green's function QED approach. *Phys. Rev. A* **2008**, *77*, 022110.